Regularized Equations for Numerical Simulation of Flows in the Two-Layer Shallow Water Approximation

T. G. Elizarova[a],* and A. V. Ivanov[b],**

[a] *Institute of Applied Mathematics, Russian Academy of Sciences, Moscow, 125047 Russia*
[b] *Faculty of Physics, Moscow State University, Moscow, 119991 Russia*
*e-mail: telizar@mail.ru
**e-mail: alexvladiv@mail.ru

Abstract—Regularized equations describing hydrodynamic flows in the two-layer shallow water approximation are constructed. A conditionally stable finite-difference scheme based on the finite-volume method is proposed for the numerical solution of these equations. The scheme is tested using several well-known one-dimensional benchmark problems, including Riemann problems.

1. INTRODUCTION

According to numerous works (see, e.g., [1–10]), the shallow water equations for two-layer flows can be written as a system of four equations (the notation used is explained in Fig. 1)

$$\frac{\partial h_1}{\partial t} + \operatorname{div}(h_1 \mathbf{u}_1) = 0, \tag{1}$$

$$\frac{\partial h_2}{\partial t} + \operatorname{div}(h_2 \mathbf{u}_2) = 0, \tag{2}$$

$$\frac{\partial (h_1 \mathbf{u}_1)}{\partial t} + \operatorname{div}(h_1 \mathbf{u}_1 \otimes \mathbf{u}_1) + \nabla \frac{g h_1^2}{2} + g h_1 \nabla (r h_2 + b) = 0, \tag{3}$$

$$\frac{\partial (h_2 \mathbf{u}_2)}{\partial t} + \operatorname{div}(h_2 \mathbf{u}_2 \otimes \mathbf{u}_2) + \nabla \frac{g h_2^2}{2} + g h_2 \nabla (h_1 + b) = 0. \tag{4}$$

Here, $h_1(\mathbf{x}, t)$ and $\mathbf{u}_1(\mathbf{x}, t)$ are the depth and velocity of the lower layer, $h_2(\mathbf{x}, t)$ and $\mathbf{u}_2(\mathbf{x}, t)$ are the depth and velocity of the upper layer, $b(\mathbf{x})$ describes the topography of the bottom, and g is the acceleration due to gravity. The layers are indexed starting from the lower one (see Fig. 1). The numerical coefficient $r = \rho_2/\rho_1 \leq 1$ is the ratio of the densities in the upper and lower layers. Obviously, for $r > 1$, Kelvin–Helmholtz instability can appear in the two-layer fluid system. The resulting flow field can no longer be described by the shallow water equations, which are derived assuming that the vertical velocity of the flow is negligibly low.

The above-written system of equations does not involve external forces (for example, wind strength or Coriolis forces) and viscous friction forces, including interlayer friction.

This system of equations represents two systems, each describing the flow of an individual layer. The layers are coupled only via the hydrostatic pressure, and this coupling is described by nonconservative nonlinear terms involving h_1 and h_2. The last circumstance leads to additional instabilities of the numerical solution as compared with the case of the single-layer equations. To overcome the arising difficulties, there are numerous techniques, including splitting approaches and kinetic algorithms and methods, in which a third (intermediate) layer of vanishing depth is introduced to stabilize the solution. Corresponding numerical algorithms and their features used to overcome specific numerical instability in the case of two-layer equations are described in [1–10] (see also references therein).
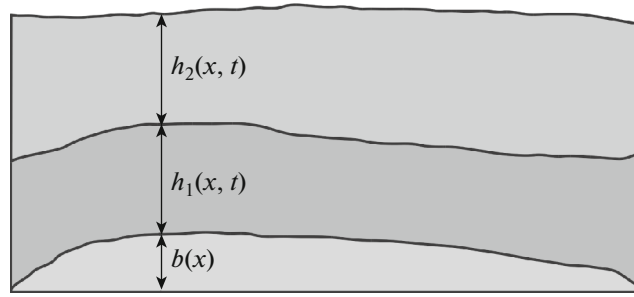
Fig. 1. Schematic view of two-layer shallow water.

Since Eqs. (1)−(4) underlying a numerical algorithm are written in nonconservative form, the resulting difference scheme is nonconservative and its limiting discontinuous solutions generally depend on the method used to specify numerical viscosity [11]. The problem of formulating the two-layer shallow water model in the form of a complete system of basis conservation laws was set up in [12], where this model was studied at the differential level. Later, this problem was addressed in a number of studies, which are overviewed in [13]. Specifically, a system of basis conservation laws consisting of the mass conservation laws in the layers, the total momentum conservation law, and the conservation law for the velocity jump at the interface of the layers was proposed in [14]. A detailed analysis of discontinuous solutions admitted by this basis system of conservation laws, including in the two-dimensional case, can be found in [15].

Numerical algorithms based on nonconservative (Eqs. (1)−(4)) and conservative (see [14]) forms of the two-layer shallow water equations are compared in Section 9. This comparison shows that both difference schemes produce similar numerical results. For this reason, our present study relies basically on an algorithm obtained by approximating the nonconservative system (1)−(4).

In this paper, for the numerical solution of the two-layer shallow water equations, we propose a new finite-difference algorithm based on the quasi-gasdynamic approach [16−18]. Previously, a numerical algorithm relying on this approach was developed for solving the shallow water equations; the algorithm was tested and found to be efficient as applied to numerous problems in the indicated approximation (see, e.g., [19−23]).

Used in this work, the method for regularizing equations aimed at the design of a stable numerical algorithm can be treated as a method of introducing artificial viscosity whose form is consistent with the features of the original system of equations and its exact solutions. Another example is the introduction of artificial viscosity approximating the physical one in fluid dynamics equations in the construction of fully conservative schemes for gas dynamics equations [24]. Kinetically consistent schemes [16] and quasi-gasdynamic equations [17, 18] can also be assigned to this class of models with additional dissipation.

The regularized form of system (1)−(4) written with the use of the quasi-gasdynamic approach is

$$\frac{\partial h_1}{\partial t} + \operatorname{div} \mathbf{j}_1 = 0, \tag{5}$$

$$\frac{\partial h_2}{\partial t} + \operatorname{div} \mathbf{j}_2 = 0, \tag{6}$$

$$\frac{\partial (h_1 \mathbf{u}_1)}{\partial t} + \operatorname{div}(\mathbf{j}_1 \otimes \mathbf{u}_1) + \nabla \frac{g h_1^2}{2} + g(h_1 - \tau_1 \operatorname{div}(h_1 \mathbf{u}_1)) \\ \times \nabla(r h_2 + b) - r g h_1 \nabla(\tau_2 \operatorname{div}(h_2 \mathbf{u}_2)) = \operatorname{div} \Pi_1, \tag{7}$$

$$\frac{\partial (h_2 \mathbf{u}_2)}{\partial t} + \operatorname{div}(\mathbf{j}_2 \otimes \mathbf{u}_2) + \nabla \frac{g h_2^2}{2} + g(h_2 - \tau_2 \operatorname{div}(h_2 \mathbf{u}_2)) \\ \times \nabla(h_1 + b) - g h_2 \nabla(\tau_1 \operatorname{div}(h_1 \mathbf{u}_1)) = \operatorname{div} \Pi_2, \tag{8}$$

where

$$\mathbf{w}_1 = \frac{\tau_1}{h_1}[\operatorname{div}(h_1 \mathbf{u}_1 \otimes \mathbf{u}_1) + g h_1 \nabla(b + h_1 + r h_2)], \tag{9}$$

$$\mathbf{j}_1 = h_1(\mathbf{u}_1 - \mathbf{w}_1), \tag{10}$$

$$\mathbf{w}_2 = \frac{\tau_2}{h_2}\left[\operatorname{div}\left(h_2\mathbf{u}_2 \otimes \mathbf{u}_2\right) + gh_2\nabla\left(b + h_1 + h_2\right)\right], \tag{11}$$

$$\mathbf{j}_2 = h_2\left(\mathbf{u}_2 - \mathbf{w}_2\right), \tag{12}$$

$$\Pi_1 = \tau_1\mathbf{u}_1 \otimes \left[h_1\left(\mathbf{u}_1 \cdot \nabla\right)\mathbf{u}_1 + gh_1\nabla\left(b + h_1 + rh_2\right)\right] + \tau_1 I\left[gh_1 \operatorname{div}\left(h_1\mathbf{u}_1\right)\right], \tag{13}$$

$$\Pi_2 = \tau_2\mathbf{u}_2 \otimes \left[h_2\left(\mathbf{u}_2 \cdot \nabla\right)\mathbf{u}_2 + gh_2\nabla\left(b + h_1 + h_2\right)\right] + \tau_2 I\left[gh_2 \operatorname{div}\left(h_2\mathbf{u}_2\right)\right]. \tag{14}$$

These equations are based on a nonconservative form of the original system (1)−(4) and are a generalization of the regularization approach developed earlier for the single-layer shallow water model [19−23].

In Section 2, we describe a method for constructing a regularized form of the two-layer shallow water equations in the one-dimensional case (referred to hereafter as the *large system*). A corresponding difference scheme is presented in Section 3. Whether the scheme is well-balanced is verified in Section 4. In Sections 5−8, we present examples of numerical computations of well-known test problems, such as interface propagation, the conventional Riemann problem, the Riemann problem near a sloping beach (in which case the so-called dry-bed effect has to be taken into account), and transcritical flows of layers over bottom irregularities.

The regularized system of shallow water equations obtained by applying the quasi-hydrodynamic approach (referred to hereafter as the *small system*) is described in the Appendix. This approach was used to compute test problems, and its features distinguishing it from the basic algorithm are indicated in the text. The computations show that the small system exhibits strong oscillations on solution discontinuities and is poorly stable when the layer densities are close in value.

2. SMOOTHED TWO-LAYER SHALLOW WATER EQUATIONS

The one-dimensional two-layer shallow water equations are given by

$$\frac{\partial h_1}{\partial t} + \frac{\partial}{\partial x}\left(h_1 u_1\right) = 0, \tag{15}$$

$$\frac{\partial h_2}{\partial t} + \frac{\partial}{\partial x}\left(h_2 u_2\right) = 0, \tag{16}$$

$$\frac{\partial\left(h_1 u_1\right)}{\partial t} + \frac{\partial\left(h_1 u_1^2\right)}{\partial x} + \frac{\partial}{\partial x}\left(\frac{gh_1^2}{2}\right) + rgh_1\frac{\partial h_2}{\partial x} + gh_1\frac{\partial b}{\partial x} = 0, \tag{17}$$

$$\frac{\partial\left(h_2 u_2\right)}{\partial t} + \frac{\partial\left(h_2 u_2^2\right)}{\partial x} + \frac{\partial}{\partial x}\left(\frac{gh_2^2}{2}\right) + gh_2\frac{\partial h_1}{\partial x} + gh_2\frac{\partial b}{\partial x} = 0. \tag{18}$$

By analogy with the construction of regularized gas dynamics equations and regularized shallow water equations, we assume that the velocity and the depth of a liquid layer change over a short time interval (smoothing time ~τ) to take new values u^* and h^*, respectively. To determine them, the corresponding functions are expanded in Taylor series up to the first term with τ:

$$u^* = u + \tau\frac{\partial u}{\partial t}, \quad h^* = h + \tau\frac{\partial h}{\partial t}. \tag{19}$$

Substituting (19) into h^*u^* and retaining only first-order terms in τ, we obtain

$$h^*u^* = \left(h + \tau\frac{\partial h}{\partial t}\right)\left(u + \tau\frac{\partial u}{\partial t}\right) = hu + \tau\frac{\partial(hu)}{\partial t} + \mathbb{O}\left(\tau^2\right).$$

An expression for the time derivative is obtained from Eqs. (17) and (18). Let us describe this procedure as applied to the regularization of the equations for the lower layer (h_1, u_1):

$$\frac{\partial\left(h_1 u_1\right)}{\partial t} = -\frac{\partial\left(h_1 u_1^2\right)}{\partial x} - \frac{\partial}{\partial x}\left(\frac{gh_1^2}{2}\right) - rgh_1\frac{\partial h_2}{\partial x} - gh_1\frac{\partial b}{\partial x}.$$

Introducing

$$w_1 = \frac{\tau_1}{h_1}\left[\frac{\partial\left(h_1 u_1^2\right)}{\partial x} + \frac{\partial}{\partial x}\left(\frac{g h_1^2}{2}\right) + r g h_1 \frac{\partial h_2}{\partial x} + g h_1 \frac{\partial b}{\partial x}\right], \tag{20}$$

$$j_1 = h_1\left(u_1 - w_1\right), \tag{21}$$

we obtain

$$\frac{\partial h_1}{\partial t} + \frac{\partial j_1}{\partial x} = 0.$$

Similarly,

$$w_2 = \frac{\tau_2}{h_2}\left[\frac{\partial\left(h_2 u_2^2\right)}{\partial x} + \frac{\partial}{\partial x}\left(\frac{g h_2^2}{2}\right) + g h_2 \frac{\partial h_1}{\partial x} + g h_2 \frac{\partial b}{\partial x}\right], \tag{22}$$

$$j_2 = h_2\left(u_2 - w_2\right),$$
$$\frac{\partial h_2}{\partial t} + \frac{\partial j_2}{\partial x} = 0. \tag{23}$$

Now, we derive an expression for each term in Eq. (17) at $h_1 = h_1^*$ and $u_1 = u_1^*$:

$$h_1^*(u_1^*)^2 = \left(h_1 + \tau_1\frac{\partial h_1}{\partial t}\right)\left(u_1 + \tau_1\frac{\partial u_1}{\partial t}\right)^2 = \left(h_1 + \tau_1\frac{\partial h_1}{\partial t}\right)\left(u_1^2 + 2 u_1 \tau_1\frac{\partial u_1}{\partial t} + \mathbb{O}(\tau_1^2)\right)$$

$$= u_1\left(h_1 u_1 + \tau_1\frac{\partial(h_1 u_1)}{\partial t}\right) + u_1 h_1 \tau_1\frac{\partial u_1}{\partial t} + \mathbb{O}(\tau^2) = J u_1 j_1 + u_1 h_1 \tau_1\frac{\partial u_1}{\partial t} + \mathbb{O}(\tau^2).$$

Using Eq. (17), we express the time derivative

$$\frac{\partial u_1}{\partial t} = -\left[u_1\frac{\partial u_1}{\partial x} + g\frac{\partial h_1}{\partial x} + r g\frac{\partial h_2}{\partial x} + g\frac{\partial b}{\partial x}\right]. \tag{24}$$

An expression for the next term is obtained using (15):

$$\frac{1}{2}g\left(h_1^*\right)^2 = \frac{1}{2}g\left(h_1 + \tau_1\frac{\partial h_1}{\partial t}\right)^2 = \frac{1}{2}g h_1^2 + g h_1 \tau_1\left[-h_1\frac{\partial u_1}{\partial x} - u_1\frac{\partial h_1}{\partial x}\right] + \mathbb{O}(\tau^2).$$

Define

$$\Pi_1 = \tau_1 u_1 h_1\left[u_1\frac{\partial u_1}{\partial x} + g\frac{\partial h_1}{\partial x} + r g\frac{\partial h_2}{\partial x} + g\frac{\partial b}{\partial x}\right] + \tau_1 g h_1\left[h_1\frac{\partial u_1}{\partial x} + u_1\frac{\partial h_1}{\partial x}\right]. \tag{25}$$

The remaining terms contain h_1^* outside the derivative and can be written as

$$h_1^* = \left(h_1 - \tau_1\frac{\partial(h_1 u_1)}{\partial x}\right).$$

At the last step, we transform the derivative $\partial h_2^*/\partial x$:

$$\frac{\partial h_2^*}{\partial x} = \frac{\partial\left(h_2 - \tau_2\dfrac{\partial(h_2 u_2)}{\partial x}\right)}{\partial x} = \frac{\partial h_2}{\partial x} - \frac{\partial}{\partial x}\left(\tau_2\frac{\partial(h_2 u_2)}{\partial x}\right).$$

Thus, taking into account the transformations described above, for Eq. (17), we obtain

$$\frac{\partial\left(h_1 u_1\right)}{\partial t} + \frac{\partial\left(u_1 j_1\right)}{\partial x} + \frac{\partial}{\partial x}\left(\frac{g h_1^2}{2}\right) + g\left(h_1 - \tau_1\frac{\partial(h_1 u_1)}{\partial x}\right)\left[\frac{\partial h_2}{\partial x} - \frac{\partial}{\partial x}\left(\tau_2\frac{\partial(h_2 u_2)}{\partial x}\right) + \frac{\partial b}{\partial x}\right] = \frac{\partial\Pi_1}{\partial x}.$$

The term

$$g\tau_1\frac{\partial(h_1 u_1)}{\partial x}\frac{\partial}{\partial x}\left(\tau_2\frac{\partial(h_2 u_2)}{\partial x}\right) = O(\tau^2)$$

is of the second order in τ, so it can be neglected.

Applying the same procedure to Eq. (18) and simplifying the resulting expressions, we obtain a system of smoothed equations for the second layer.

Thus, we have constructed the following regularized system for the two-layer shallow water equations, which is a special case of system (5)−(14):

$$\frac{\partial h_1}{\partial t} + \frac{\partial j_1}{\partial x} = 0, \tag{26}$$

$$\frac{\partial h_2}{\partial t} + \frac{\partial j_2}{\partial x} = 0, \tag{27}$$

$$\frac{\partial (h_1 u_1)}{\partial t} + \frac{\partial (u_1 j_1)}{\partial x} + \frac{\partial}{\partial x}\left(\frac{g h_1^2}{2}\right) + g\left(h_1 - \tau_1 \frac{\partial (h_1 u_1)}{\partial x}\right)\left[r\frac{\partial h_2}{\partial x} + \frac{\partial b}{\partial x}\right] - rgh_1\frac{\partial}{\partial x}\left(\tau_2 \frac{\partial (h_2 u_2)}{\partial x}\right) = \frac{\partial \Pi_1}{\partial x}, \tag{28}$$

$$\frac{\partial (h_2 u_2)}{\partial t} + \frac{\partial (u_2 j_2)}{\partial x} + \frac{\partial}{\partial x}\left(\frac{g h_2^2}{2}\right) + g\left(h_2 - \tau_2 \frac{\partial (h_2 u_2)}{\partial x}\right)\left[\frac{\partial h_1}{\partial x} + \frac{\partial b}{\partial x}\right] - gh_2\frac{\partial}{\partial x}\left(\tau_1 \frac{\partial (h_1 u_1)}{\partial x}\right) = \frac{\partial \Pi_2}{\partial x}, \tag{29}$$

where

$$w_1 = \frac{\tau_1}{h_1}\left[\frac{\partial (h_1 u_1^2)}{\partial x} + gh_1\frac{\partial}{\partial x}(h_1 + rh_2 + b)\right], \tag{30}$$

$$j_1 = h_1(u_1 - w_1), \tag{31}$$

$$w_2 = \frac{\tau_2}{h_2}\left[\frac{\partial (h_2 u_2^2)}{\partial x} + gh_2\frac{\partial}{\partial x}(h_1 + h_2 + b)\right], \tag{32}$$

$$j_2 = h_2(u_2 - w_2), \tag{33}$$

$$\Pi_1 = u_1 h_1 \tau_1\left[u_1\frac{\partial u_1}{\partial x} + g\frac{\partial}{\partial x}(h_1 + rh_2 + b)\right] + gh_1\tau_1\frac{\partial (h_1 u_1)}{\partial x}, \tag{34}$$

$$\Pi_2 = u_2 h_2 \tau_2\left[u_2\frac{\partial u_2}{\partial x} + g\frac{\partial}{\partial x}(h_1 + h_2 + b)\right] + gh_2\tau_2\frac{\partial (h_2 u_2)}{\partial x}. \tag{35}$$

3. DIFFERENCE SCHEME

By analogy with the algorithms from [19, 20] developed for quasi-gasdynamic equations, for the numerical solution of regularized equations (26)−(35), we use a time-explicit difference scheme with all spatial derivatives approximated by central differences.

The desired variables $h_1(x,t)$, $h_2(x,t)$, $u_1(x,t)$, $u_2(x,t)$ are specified at nodes of a spatial grid i. The values of the variables at half-integer spatial points $i + 1/2$ are calculated as the arithmetic mean of the values at neighboring points:

$$b_{i+1/2} = \frac{b_i + b_{i+1}}{2}, \quad (\tau_l)_{i+1/2} = \frac{(\tau_l)_i + (\tau_l)_{i+1}}{2},$$

$$(h_l)_{i+1/2} = \frac{(h_l)_i + (h_l)_{i+1}}{2}, \quad (u_l)_{i+1/2} = \frac{(u_l)_i + (u_l)_{i+1}}{2}, \quad l = 1, 2.$$

Then, if Δt and Δx are the time and coordinate step sizes, respectively, we obtain

$$(w_1)_{i+1/2} = \frac{(\tau_1)_{i+1/2}}{(h_1)_{i+1/2}}\left(\frac{(h_1 u_1^2)_{i+1} - (h_1 u_1^2)_i}{\Delta x} + g(h_1)_{i+1/2}\frac{(h_1)_{i+1} + r(h_2)_{i+1} + b_{i+1} - (h_1)_i - r(h_2)_i - b_i}{\Delta x}\right), \tag{36}$$

$$(w_2)_{i+1/2} = \frac{(\tau_2)_{i+1/2}}{(h_2)_{i+1/2}}\left(\frac{(h_2 u_2^2)_{i+1} - (h_2 u_2^2)_i}{\Delta x} + g(h_2)_{i+1/2}\frac{(h_1)_{i+1} + (h_2)_{i+1} + b_{i+1} - (h_1)_i - (h_2)_i - b_i}{\Delta x}\right). \tag{37}$$

Similarly, we define

$$(\Pi_1)_{i+1/2} = (\tau_1)_{i+1/2}(u_1)_{i+1/2}(h_1)_{i+1/2}\left((u_1)_{i+1/2}\frac{(u_1)_{i+1} - (u_1)_i}{\Delta x} + g\frac{(h_1)_{i+1} + r(h_2)_{i+1} + b_{i+1} - (h_1)_i - r(h_2)_i - b_i}{\Delta x}\right)$$
$$+ g(h_1)_{i+1/2}(\tau_1)_{i+1/2}\frac{(h_1)_{i+1}(u_1)_{i+1} - (h_1)_i(u_1)_i}{\Delta x}, \tag{38}$$

$$(\Pi_2)_{i+1/2} = (\tau_2)_{i+1/2}(u_2)_{i+1/2}(h_2)_{i+1/2}\left((u_2)_{i+1/2}\frac{(u_2)_{i+1} - (u_2)_i}{\Delta x} + g\frac{(h_1)_{i+1} + (h_2)_{i+1} + b_{i+1} - (h_1)_i - (h_2)_i - b_i}{\Delta x}\right)$$
$$+ g(h_2)_{i+1/2}(\tau_2)_{i+1/2}\frac{(h_2)_{i+1}(u_2)_{i+1} - (h_2)_i(u_2)_i}{\Delta x}. \tag{39}$$

Then

$$(j_1)_{i+1/2} = (h_1)_{i+1/2}\left((u_1)_{i+1/2} - (w_1)_{i+1/2}\right), \tag{40}$$

$$(j_2)_{i+1/2} = (h_2)_{i+1/2}\left((u_2)_{i+1/2} - (w_2)_{i+1/2}\right). \tag{41}$$

By using (26), (27), (40), and (41), the first equations are approximated as

$$\frac{(h_1)_i^{k+1} - (h_1)_i^k}{\Delta t} + \frac{(j_1)_{i+1/2} - (j_1)_{i-1/2}}{\Delta x} = 0, \tag{42}$$

$$\frac{(h_2)_i^{k+1} - (h_2)_i^k}{\Delta t} + \frac{(j_2)_{i+1/2} - (j_2)_{i-1/2}}{\Delta x} = 0. \tag{43}$$

Introducing $s_l = \dfrac{\partial(h_l u_l)}{\partial x}$, we approximate the flux derivatives:

$$(s_1)_{i+1/2} = \frac{(h_1)_{i+1}(u_1)_{i+1} - (h_1)_i(u_1)_i}{\Delta x}, \tag{44}$$

$$(s_2)_{i+1/2} = \frac{(h_2)_{i+1}(u_2)_{i+1} - (h_2)_i(u_2)_i}{\Delta x}. \tag{45}$$

Equations (28) and (29) are approximated as follows:

$$\frac{(h_1)_i^{k+1}(u_1)_i^{k+1} - (h_1)_i^k(u_1)_i^k}{\Delta t} + \frac{(u_1)_{i+1/2}(j_1)_{i+1/2} - (u_1)_{i-1/2}(j_1)_{i-1/2}}{\Delta x} + \frac{g}{2}\frac{((h_1)_{i+1/2})^2 - ((h_1)_{i-1/2})^2}{\Delta x}$$
$$+ rg(h_1^*)_i\frac{(h_2)_{i+1/2} - (h_2)_{i-1/2}}{\Delta x} - rg(h_1^{**})_i\frac{(s_2)_{i+1/2}(\tau_2)_{i+1/2} - (s_2)_{i-1/2}(\tau_2)_{i-1/2}}{\Delta x} \tag{46}$$
$$+ g(h_1^*)_i\frac{b_{i+1/2} - b_{i-1/2}}{\Delta x} = \frac{(\Pi_1)_{i+1/2} - (\Pi_1)_{i-1/2}}{\Delta x},$$

$$\frac{(h_2)_i^{k+1}(u_2)_i^{k+1} - (h_2)_i^k(u_2)_i^k}{\Delta t} + \frac{(u_2)_{i+1/2}(j_2)_{i+1/2} - (u_2)_{i-1/2}(j_2)_{i-1/2}}{\Delta x} + \frac{g}{2}\frac{((h_2)_{i+1/2})^2 - ((h_2)_{i-1/2})^2}{\Delta x}$$
$$+ g(h_2^*)_i\frac{(h_1)_{i+1/2} - (h_1)_{i-1/2}}{\Delta x} - g(h_2^{**})_i\frac{(s_1)_{i+1/2}(\tau_1)_{i+1/2} - (s_1)_{i-1/2}(\tau_1)_{i-1/2}}{\Delta x} \tag{47}$$
$$+ g(h_2^*)_i\frac{b_{i+1/2} - b_{i-1/2}}{\Delta x} = \frac{(\Pi_2)_{i+1/2} - (\Pi_2)_{i-1/2}}{\Delta x}.$$

Here,

$$(h_l^*)_i = (h_l^{**})_i - (\tau_l)_i\frac{(h_l)_{i+1/2}(u_l)_{i+1/2} - (h_l)_{i-1/2}(u_l)_{i-1/2}}{\Delta x}, \quad l = 1, 2. \tag{48}$$

The terms with h_1^{**} and h_2^{**} and with h_1^* and h_2^* in Eqs. (28) and (29), respectively, can be approximated in a different manner. It will be shown in the next section that the method for the approximation of these quantities affects the accuracy to which the hydrostatic equilibrium condition is satisfied. We will use the following two approximation methods.

Method 1:

$$(h_l^{**})_i = \frac{(h_l)_{i+1/2} + (h_l)_{i-1/2}}{2}, \quad l = 1, 2. \tag{49}$$

Method 2:

$$(h_l^{**})_i = (h_l)_i, \quad l = 1, 2. \tag{50}$$

The stability of the numerical algorithm is ensured by terms with the coefficient τ. The regularizer τ is defined with the help of two independent coefficients τ_1 and τ_2 for each layer, respectively:

$$\tau_1 = \alpha_1 \frac{\Delta x}{c_1}, \quad c_1 = \sqrt{gh_1}, \tag{51}$$

$$\tau_2 = \alpha_2 \frac{\Delta x}{c_2}, \quad c_2 = \sqrt{gh_2}. \tag{52}$$

The quantity τ_i is proportional to the spatial mesh size Δx with a coefficient α_i, where $0 < \alpha_i < 1$ is a number determined by the accuracy and stability conditions. The stability condition is the Courant one, where the time step is given by the formula

$$\Delta t = \beta \left(\frac{\Delta x}{c} \right)_{\min} \tag{53}$$

A sufficient condition for the linear stability of the difference scheme for shallow water equations of form (53) was obtained in [22].

The boundaries of the computational domain are placed at half-integer points. In difference form, the boundary conditions are set with the use of dummy nodes and a second-order accurate approximation.

4. HYDROSTATIC EQUILIBRIUM CONDITIONS

To represent the numerical results in a more convenient form, we introduce the following notation:

$$\xi_1(x, t) = h_1(x, t) + b(x), \tag{54}$$

$$\xi_2(x, t) = h_2(x, t) + h_1(x, t) + b(x). \tag{55}$$

Additionally, if $\alpha_1 = \alpha_2$, for convenience, we will use

$$\alpha_1 = \alpha_2 = \alpha. \tag{56}$$

The algorithm is said to satisfy the hydrostatic equilibrium condition, which, in this context, means that the algorithm is well-balanced if, in the absence of external forces, horizontal liquid layers that are initially at rest cannot spontaneously begin to move over a rough bottom.

For the two-layer shallow water equations, this condition has the form

$$h_2 = \text{const}, \quad h_1 + b = \text{const}, \quad u_1 = u_2 = 0$$

and is checked by directly substituting these expressions into the two-layer shallow water equations and their regularized counterpart. The hydrostatic equilibrium is one of a few simple analytical solutions of the two-layer shallow water equations.

For numerical algorithms intended for solving the two-layer problem, whether this condition is satisfied depends on the numerical algorithm used. Approaches to ensuring the fulfillment of this condition are rather expensive and can be found, for example, in [1, 2].

For Method 1 (see (49)), this condition is precisely satisfied by the difference scheme, which can be checked by direct substitution of the discrete solution $(u_1)_i = (u_2)_i = 0$, $(h_1)_i + b_i = \text{const}$, $(h_2)_i = \text{const}$ into the system of difference equations (36)–(47) for the stationary problem. A similar condition was checked for the single-layer case in [19].

For Method 2 (see (50)), the substitution of the hydrostatic equilibrium condition into scheme (36)–(47) leads to relations of the form

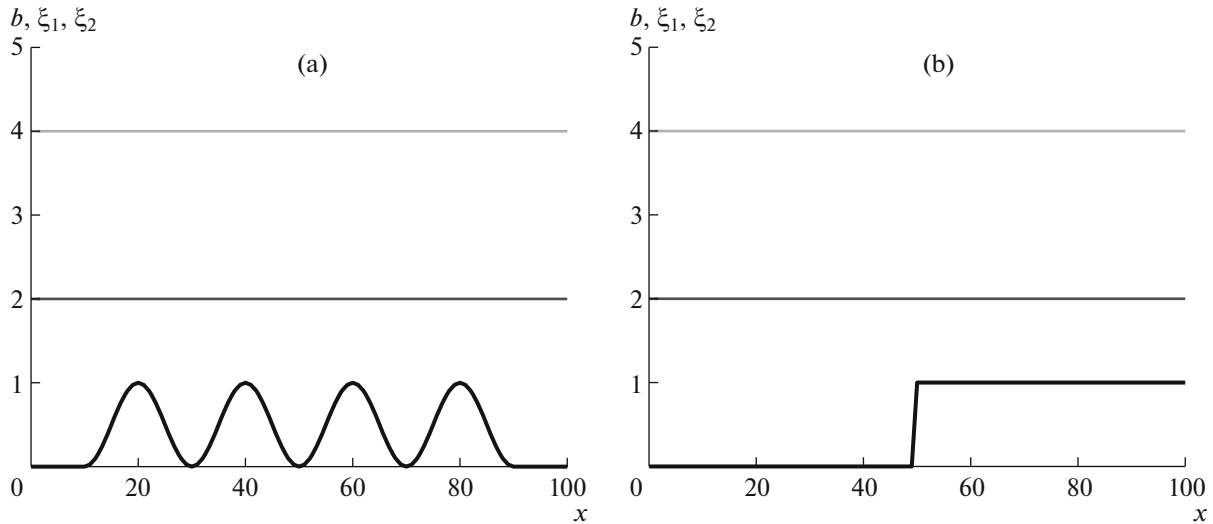$$(h_l)_i = \frac{(h_l)_{i+1/2} + (h_l)_{i-1/2}}{2}, \quad l = 1, 2.$$

Fig. 2. Method 1: hydrostatic equilibrium condition for $N = 100$ in the case of (a) smooth bottom and (b) discontinuous bottom.

To numerically verify the hydrostatic equilibrium condition as applied to a two-layer fluid, we used two problems with initial conditions

$$h_2(x, t = 0) = \text{const} = 2,$$

$$h_1(x, t = 0) + b(x) = \text{const} = 2,$$

$$u_1(x, t = 0) = u_2(x, t = 0) = 0,$$

for two cases of bottom topography, namely, the smooth profile

$$b(x) = \begin{cases} 0.5(\cos(0.1\pi x) + 1), & 10 \leqslant x \leqslant 90, \\ 0, & x < 10 \cup x > 90, \end{cases}$$

and the steplike discontinuous profile

$$b(x) = \begin{cases} 0, & x < 50 \\ 1, & x \geq 50. \end{cases}$$

The computation was performed with constant coefficients $r = 0.5$, $\beta = 0.1$, and $\alpha = 0.3$ on a grid with $N = 100$. In all the subsequent computations, we used $\beta = 0.1$. A decrease in this coefficient leads to finer grids in time, but they were not required in the tests described below. The above value of α ensures the highest stability for the regularized system [19], although the hydrostatic equilibrium condition is obviously satisfied for any values of these coefficients. The computation time was $t = 1$.

For Method 1, the numerical results are shown in Fig. 2. In this case, the numerical error for the problems with a smooth and discontinuous bottom can be regarded as equal to machine zero, namely, about $10^{-15}-10^{-16}$.

For Method 2, the numerical results are presented in Fig. 3. It can be seen that the equilibrium condition is satisfied approximately. The tables give the maximum peaks observed in the computations based on this method. For the problem with a smooth bottom, the results in Table 1 suggest that the solution

Table 1. Smooth bottom

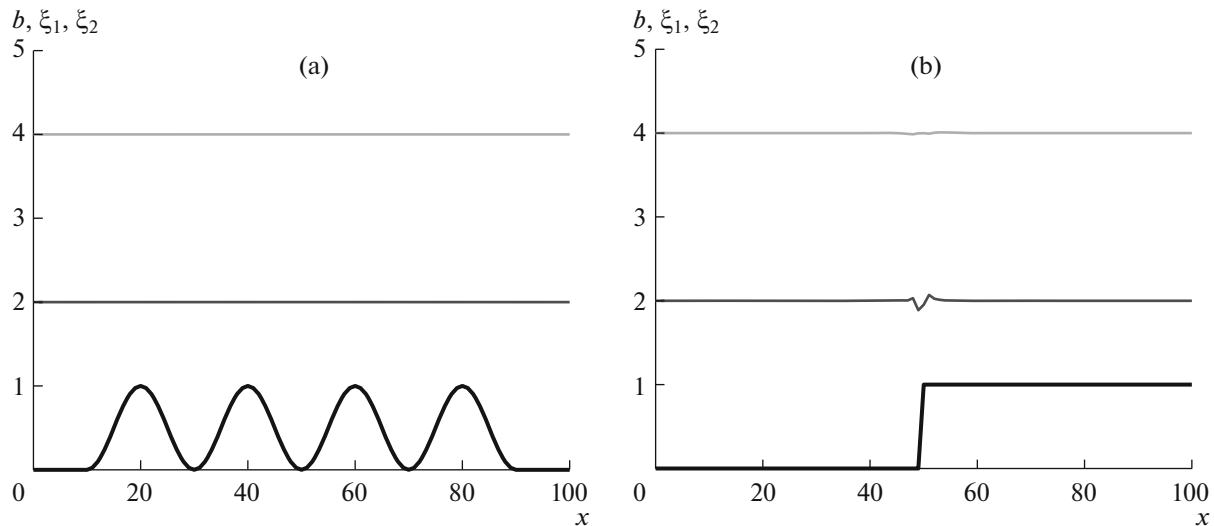|	$N = 100$	$N = 200$	$N = 500$	$N = 1000$
h_1	1.68×10^{-3}	4.96×10^{-4}	8.42×10^{-5}	2.16×10^{-5}
h_2	5.53×10^{-4}	1.68×10^{-4}	3.15×10^{-5}	8.25×10^{-6}

Fig. 3. Method 2: hydrostatic equilibrium condition for $N = 100$ in the case of (a) smooth bottom and (b) discontinuous bottom.

converges rapidly with decreasing mesh size. For the problem with a discontinuous bottom profile (Table 2), this convergence is not observed.

In the subsequent computations, we used Method 1, which is a well-balanced solver.

5. TEST 1: PROPAGATION OF AN INTERFACE WITH DISCONTINUITY

This test was investigated in detail in [1–4]. Its formulation is based on [1]. Consider a system with a flat bottom ($b(x) = 0$) in which $g = 9.81$, $r = 0.98$, and the initial depths of the layers are given by

$$h_2(x, t = 0) = \begin{cases} 0.5, & x < 0.5, \\ 0.55, & x \geqslant 0.5, \end{cases}$$

$$h_1(x, t = 0) = \begin{cases} 0.5, & x < 0.5, \\ 0.45, & x \geqslant 0.5, \end{cases}$$

$$u_1(x, t = 0) = u_2(x, t = 0) = 2.5.$$

In [1] this problem was solved for $x \in [0,1]$ with the number of cells being $N = 100$; the results were demonstrated for the time $t = 0.05$. To solve the problem, the authors of [1] developed stable first- and second-order accurate time-splitting schemes, which are *well-balanced* and satisfy a discrete entropy inequality.

Figure 4 shows the results obtained at the same time with use of the regularized shallow water equations for $N = 100$ and $\alpha = 0.3$.

Figure 5 presents the numerical solution for various values of the regularization coefficient α ($N = 100$). As $\alpha = 0.05$ is approached, oscillations arise in the numerical solution and it becomes unstable. These results agree with [19].

According to the authors of [1], the numerical solution near the front exhibits oscillations, which can be seen on a zoomed fragment of the figure in x. However, these oscillations are small against the back-

Table 2. Bottom with discontinuity

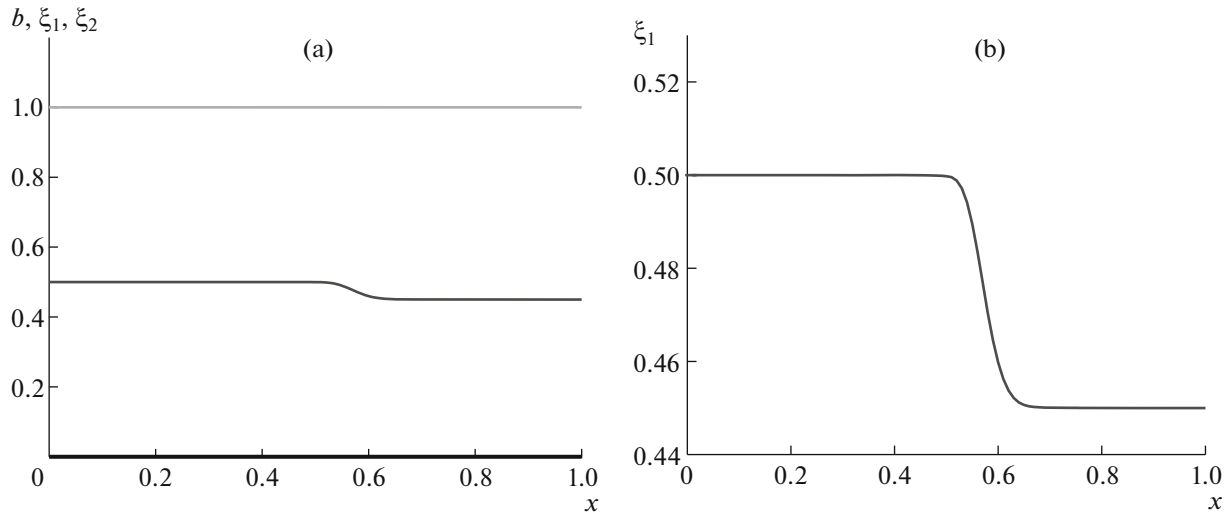|	$N = 100$	$N = 200$	$N = 500$	$N = 1000$
h_1	0.13	0.16	0.15	0.14
h_2	0.025	0.025	0.021	0.021

Fig. 4. Test 1, $N = 100$, $\beta = 0.1$, $\alpha = 0.3$: (a) whole field and (b) a fragment of the profile.
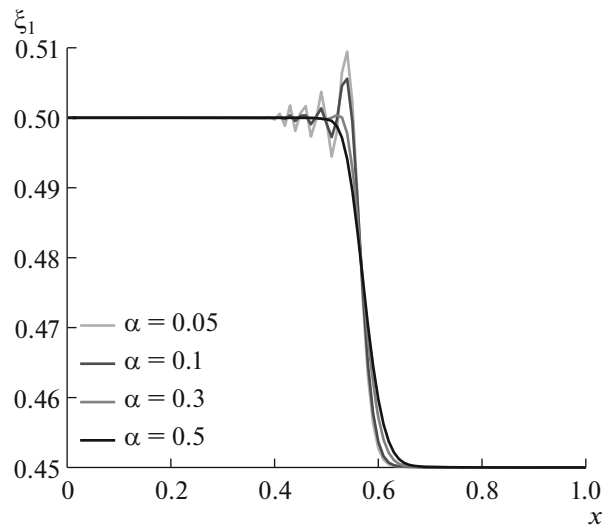

Fig. 5. Test 1: ξ_1 for various α and $N = 100$.

ground field, they are observed for $x \in [0.5, 0.6]$, and their amplitude is about 0.01 for the first-order accurate scheme and 0.003 for the second-order accurate scheme. An analysis of the results suggests that the oscillations obtained in our computations in the zone $x \in [0.5, 0.6]$ for $\alpha = 0.1$ nearly coincide in amplitude with the oscillations of the second-order solution produced in [1].

It was indicated in [2] that insufficient numerical viscosity in this problem may lead to additional interface instabilities, which become more noticeable with a larger number of grid points. At the time $t = 0.05$, such high-frequency instability occurs ahead of the front near the point 0.4. The same oscillations were observed when this problem was computed using the quasi-hydrodynamic (small) system of two-layer shallow water equations. The interface oscillations suggest the lack of smoothing in the small system of equations. The numerical experiments have shown that the quasi-gasdynamic (large) system is much more stable than the small one and its numerical solution does not exhibit the indicated instabilities.

Fine Grid Computations

Numerical experiments show that the asymptotic solution of the problem for large N is a step at the front. This is demonstrated in Fig. 6a. For $N = 5000$ and 10000, it can be clearly seen that both front segments bifurcate and flatten. In [1] only $N = 100$ was considered and this phenomenon was not observed.
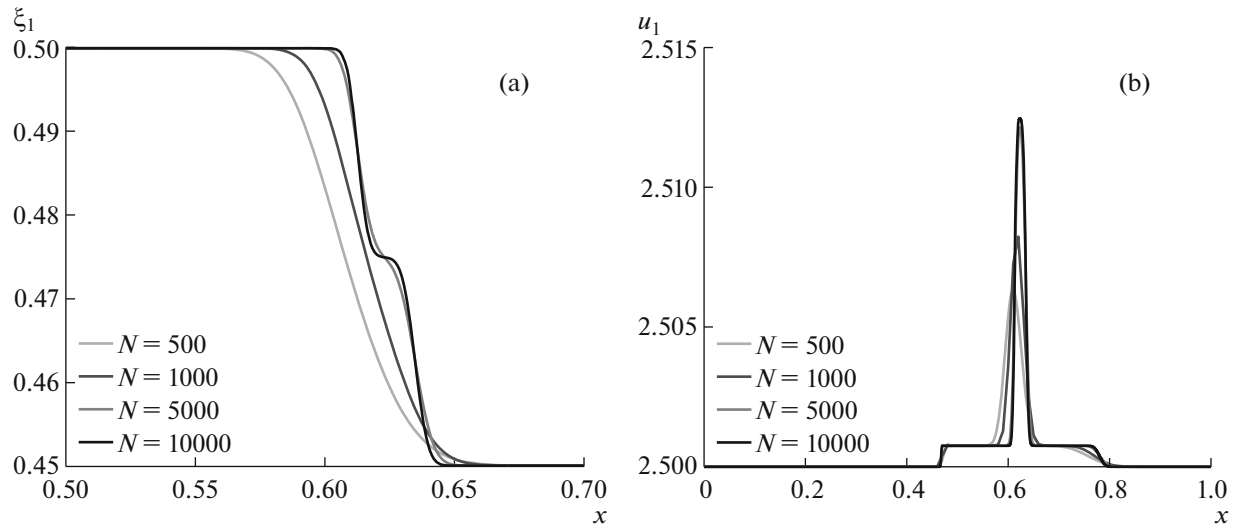
Fig. 6. Test 1: (a) ξ_1 and (b) u_1 for $g = 10$, $\alpha = 0.5$, and various N.

The bifurcation of the front and the formation of a step were obtained in [2] for $N = 10\,000$. Note that the problem in [2] was considered for $g = 10$ (which was taken into account in our computation) and, additionally, a relaxation method with various artificial viscosity was used. The results presented in Fig. 6 ($\alpha = 0.5$) agree well with those of [2].

In the case of the small system, the bifurcation of the interface jump front was also observed on a finer spatial grid ($N = 10\,000$).

Values of r Close to 1

It was noted in [1] that the schemes used here begins to diverge as $r = \rho_2/\rho_1 \to 1$. This can be explained from a physical point of view: for $r > 1$, the heavier layer overlies the lighter one, so the fluids intermix, which is manifested as strong numerical oscillations at the interface and, as a consequence, leads to the divergence of the scheme.

It was shown in [26] that a similar effect is observed with the use of the regularized two-layer shallow water equations. The stability of difference schemes as $r = \rho_2/\rho_1 \to 1$ is an important factor in the computation of liquid layers with slightly different densities.

6. TEST 2: RIEMANN PROBLEM FOR VARIOUS r

This test was described and studied in [1]. Consider a system with a flat bottom ($b(x) = 0$) in which $g = 9.81$ and

$$h_1(x, t = 0) = \begin{cases} 0.2, & x < 5, \\ 1.8, & x \geqslant 5, \end{cases}$$

$$h_2(x, t = 0) + h_1(x, t = 0) = 2,$$
$$u_1(x, t = 0) = u_2(x, t = 0) = 0.$$

The number of grid points was $N = 500$ over the interval $x \in [0, 10]$; the results were presented for $t = 1$. In [1] the problem was solved using first- and second-order accurate hydrostatic solvers and a kinetic solver, which is considered more accurate and stable.

For the large system in this and the subsequent tests, we used an optimal value of the regularization coefficient, namely, $\alpha = 0.5$. Throughout the rest of this paper, we mean this value, unless otherwise stated.
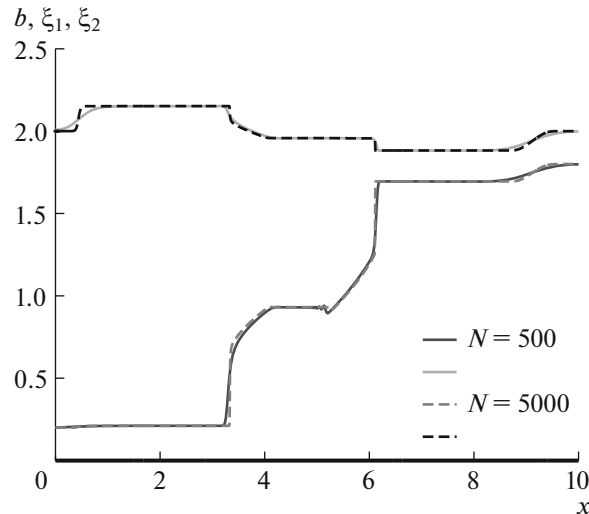
Fig. 7. Test 2: layer depth distribution for $r = 0.7$, $t = 1$, $\alpha = 0.5$, $\beta = 0.1$, and various N.

Variant $r = 0.7$

This case is shown in Fig. 7 at $t = 1$. Our results are similar to those of [1] produced by the second-order hydrostatic solver. As in [1], the lower layer distribution has plateaus at a depth of $h_1 = 1$: $x \in [4, 5.5]$ and, then, at $h_1 = 1.75$: $x \in [6, 9]$. Similarly, the upper layer has three noticeable plateaus over $x \in [0, 3]; [4, 6]; [6, 9]$, respectively.

The dependence of the solution on α was analyzed. For $\alpha \leqslant 0.05$, the solution began to oscillate and diverged. A comparison of the solutions from [1] with those based on the large system with $N = 500$ and 5000 showed that they agree very well even on grids with identical numbers of nodes. Figure 7 demonstrates the grid convergence of the numerical solution.

Note that this problem was solved using a first-order accurate difference scheme with a Courant number being 10 times higher than that in [1].

As was noted in [1], the solution produced by the first-order hydrostatic solver exhibits unphysical discontinuities. At the same time, the more universal and more stable kinetic solver of the first order yields an unphysical extremely smoothed solution. An adequate numerical solution is obtained only by applying the second-order accurate hydrostatic or kinetic solvers.

Variant $r = 0.98$

In [1] this problem was simulated for r close to 1 ($\rho_2/\rho_1 = 0.98$). The authors of [1] note that, in this case, a stationary discontinuity is formed, whose shape depends significantly on the solver used. In our computations, the solution obtained using the large system differs widely from that in [1]. This case is discussed in more detail in [26].

Variant $r = 1$

The partition was specified by $N = 500$. Figure 8a presents a stable structure of the layers for $r = 1$. For $\alpha = 0.3$, this structure remains nearly unchanged over time (the front bifurcates at $t > 5$). This result seems natural and physical, since the case of a stationary discontinuity at $r = 1$ corresponds to a stationary fluid an everywhere identical density. Note that the proposed algorithm turns out to be stable for this specific limiting case.

As $r > 1$ increases slightly, the numerical solution becomes unstable, which is clearly seen in Fig. 8b ($\alpha = 0.5$). For $r > 1.0005$ and $t > 1$, the scheme diverges. This, in turn, suggests that the result agrees with the physical instability of such layers.
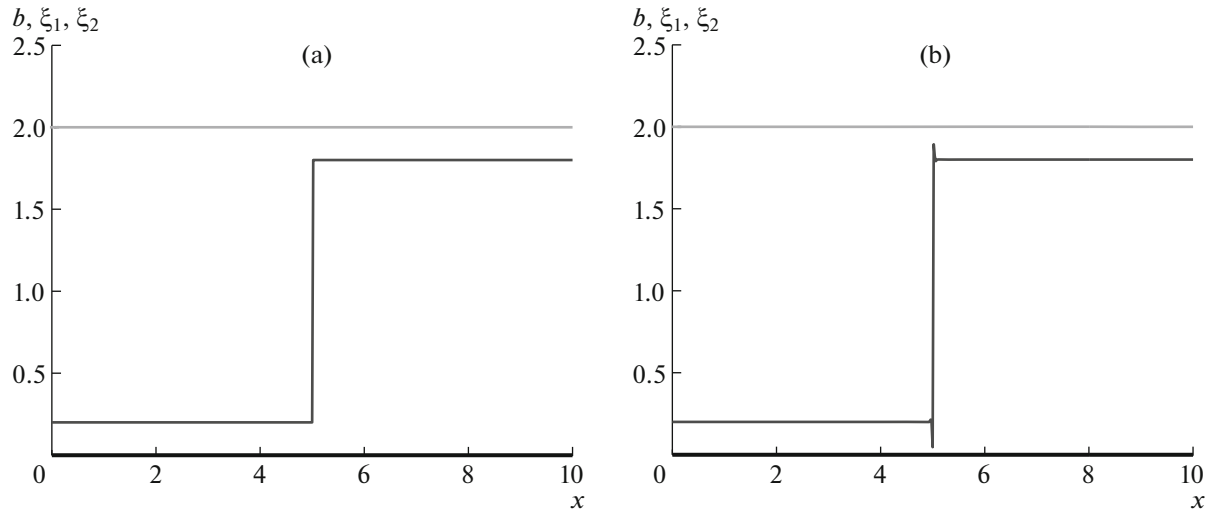
Fig. 8. Test 2, $N = 500$, $\beta = 0.1$: (a) $r = 1.0$, $\alpha = 0.3$, and $t = 5$ and (b) $r = 1.0005$, $\alpha = 0.5$, and $t = 1$.

7. TEST 3: RIEMANN PROBLEM NEAR A SLOPING BEACH

In [1] this test was considered with $g = 9.81$, $r = 0.95$, $x \in [0,10]$, and the initial conditions

$$h_1(x, t = 0) = \begin{cases} 0.5, & x < 0.25, \\ 0, & x \geqslant 0.25, \end{cases}$$

$$h_2(x, t = 0) = (1 - h_1(x, t = 0) - b(x))_+,$$
$$u_1(x, t = 0) = u_2(x, t = 0) = 0,$$

for $N = 100$. The results were presented for $t = 0.5$ and $t = 50$.

In [1] this problem was solved using a kinetic solver. The solid wall boundary condition was used on the left to ensure mass conservation. The system in void regions (i.e., dry-bed zones) was found to behave well. It was shown that a stable equilibrium is reached (by $t = 50$), which suggests that the solver of [1] is well-balanced.

In the present paper, to solve this problem, the boundary conditions of system (36)−(47) were supplemented by dry-bed conditions. Specifically, following [20], a small ε was chosen such that

$$(\tau_1)_i = \begin{cases} \alpha \dfrac{\Delta x}{\sqrt{g((h_1)_i)}}, & (h_1)_i > \varepsilon, \\ 0, & (h_1)_i \leqslant \varepsilon, \end{cases}$$

$$(\tau_2)_i = \begin{cases} \alpha \dfrac{\Delta x}{\sqrt{g((h_2)_i)}}, & (h_2)_i > \varepsilon, \\ 0, & (h_2)_i \leqslant \varepsilon, \end{cases}$$

and

$$(u_1)_i^{k+1} = \begin{cases} (46), & (h_1)_i^{k+1} > \varepsilon, \\ 0, & (h_1)_i^{k+1} \leqslant \varepsilon, \end{cases}$$

$$(u_2)_i^{k+1} = \begin{cases} (47), & (h_2)_i^{k+1} > \varepsilon, \\ 0, & (h_2)_i^{k+1} \leqslant \varepsilon. \end{cases}$$
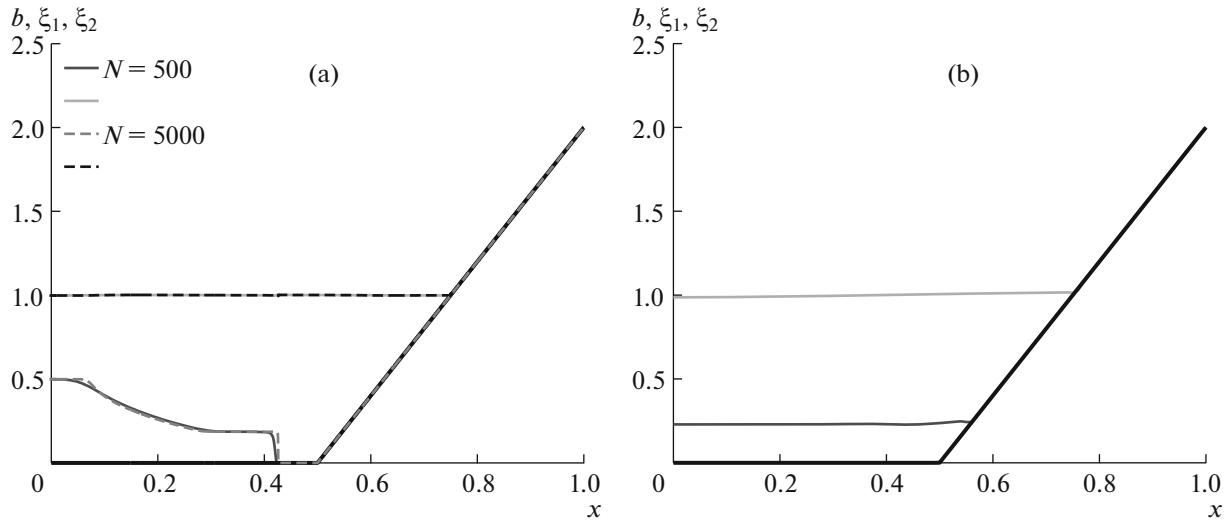
Fig. 9. Test 3, $\beta = 0.1$, $\alpha = 0.5$: (a) $t = 0.5$ for various N and (b) $t = 50$, $N = 100$.

For this problem, the cutoff parameter was specified as $\varepsilon = 0.01$. As ε was decreased, the time step had to be reduced to ensure stable computation of the problem. To smooth the solution in front propagation over a dry bed, we introduced additional dissipation of the form

$$(\Pi_{NS})_i = \tau_i \frac{gh_i^2}{2} \frac{\partial u_i}{\partial x}, \quad i = 1, 2. \tag{57}$$

This additional dissipation has the form of Navier–Stokes viscosity [24].

To compare the results with [1], the test was run with the same partition $N = 100$ (Fig. 9). Under mesh refinement at $t = 0.5$, we obtained a conventional decay of a discontinuity, which can be observed in Fig. 9a. At the time $t = 50$, the front position and the depths of the layers agree well with the reference data from [1].

Thus, we can conclude that the large system agrees, in accuracy, with the second-order accurate hydrostatic solver from [1], while being able to solve problems addressed with a more stable second-order accurate kinetic solver.

8. TEST 4: TRANSCRITICAL FLOW OVER BOTTOM IRREGULARITIES

The next problem was taken from [2]. Namely, we considered the transcritical flow connecting two infinite reservoirs with a Froude number varying from values smaller than 1 to supercritical values reached at the crest. Depending on the initial and boundary conditions, the solution exhibits or does not exhibit a steady-state discontinuity, i.e., a hydraulic jump.

The problem was considered with the following conditions:

$$x \in [-3, 3], \quad g = 10, \quad r = 0.98,$$

$$b(x) = \begin{cases} 0.125\left(\cos\frac{\pi}{2}x + 1\right), & |x| \leq 2, \\ 0, & 2 < |x| \leq 3. \end{cases}$$

Note that the shallow water equations (15)–(18) have the exact solution

$$\begin{cases} Q_1 = h_1 u_1 = \text{const}_1, & \dfrac{Q_1^2}{2gh_1^2} + h_1 + rh_2 + b = \text{const}_2, \\[3mm] Q_2 = h_2 u_2 = \text{const}_3, & \dfrac{Q_2^2}{2gh_2^2} + h_1 + h_2 + b = \text{const}_4. \end{cases} \tag{58}$$

Two tests were considered in [2], namely, the case of parallel flows and the case of layers flowing in opposite directions. Both cases are described by system (58).

Consider parallel flows. The boundary condition imposed on the left is

$$h_i u_i\big|_{x=-3} = (Q_i)_{\text{in}} = \text{const}, \quad \frac{\partial h_i}{\partial x}\bigg|_{x=-3} = 0, \quad i = 1, 2; \tag{59}$$

and the flow drift condition is set on the right:

$$\frac{\partial h_i}{\partial x}\bigg|_{x=3} = 0, \quad \frac{\partial u_i}{\partial x}\bigg|_{x=3} = 0, \quad i = 1, 2, \tag{60}$$

here,

$$(Q_1)_{\text{in}} = (Q_2)_{\text{in}} = 0.09282893.$$

Parallel Flows without Discontinuity

For the problem without discontinuity, the initial conditions were specified as

$$h_i(x, 0) = \begin{cases} (h_i)_{\text{in}}, & -3 < x < -2, \\ A\cos(0.25\pi(x+2)) + B, & -2 \leqslant x \leqslant 2, \\ (h_i)_{\text{out}}, & 2 < x < 3, \end{cases} \tag{61}$$

$$h_i(x, 0)u_i(x, 0) = Q_i(x) = (Q_i)_{\text{in}},$$

where

$$A = 0.5\big((h_i)_{\text{in}} - (h_i)_{\text{out}}\big), \quad B = 0.5\big((h_i)_{\text{in}} + (h_i)_{\text{out}}\big), \quad i = 1, 2. \tag{62}$$

The numbers $(h_i)_{\text{in}}$ and $(h_i)_{\text{out}}$ were taken arbitrary, but close to the final result. We used the results from [2] and Eqs. (58) describing the exact solution. Thus,

$$(h_1)_{\text{in}} = 1.0816731, \quad (h_1)_{\text{out}} = 0.1616669,$$

$$(h_2)_{\text{in}} = 0.4311358, \quad (h_2)_{\text{out}} = 1.3338331.$$

Following [2, 3], the transcriticality of the flow was determined using the "combined" Froude number G defined as

$$G^2 = Fr_1^2 + Fr_2^2 - (1 - r)Fr_1^2 Fr_2^2, \tag{63}$$

where Fr_i, $i = 1, 2$, are the Froude numbers for layers 1 and 2, which are calculated as

$$Fr_i^2 = \frac{u_i^2}{g' h_i}, \quad g' = (1 - r)g. \tag{64}$$

The flow is subcritical for $G^2 < 1$ and transcritical for $G^2 > 1$.

The distribution of the liquid layers and the Froude numbers at $t = 300$ are shown in Fig. 10. It can be seen that the solution varies insignificantly under mesh refinement, which suggests that the required accuracy was reached. Moreover, it can be seen that the flow is transcritical: as it goes over the bump on the bottom surface, the velocity grows and the combined Froude number passes through unity.

It should also be noted that the solution agrees with the result of the source, where the final boundary values for the depths were

$$h_1\big|_{x=-3} = 1.0816731, \quad h_1\big|_{x=3} = 0.1616669,$$

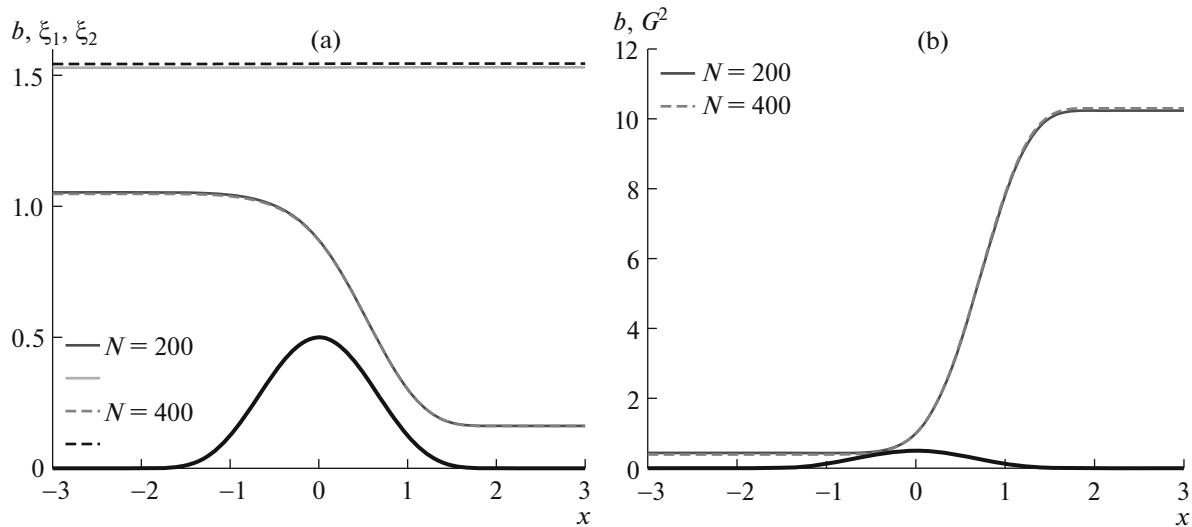$$h_2\big|_{x=-3} = 0.4311358, \quad h_2\big|_{x=3} = 1.3338331.$$

Fig. 10. Test 4, large system, flow without discontinuity for various N, $\alpha = 0.5$, $\beta = 0.1$, and $t = 300$: (a) layer depth distribution and (b) Froude number with schematic bottom topography.

Parallel Flows with Discontinuity

The initial conditions were specified as layers at rest, which was necessary for the formation of a hydraulic jump:

$$h_1(x,0) + b(x) = 0.9205217, \quad h_2(x,0) = 0.5794783,$$

$$u_1(x,0) = u_2(x,0) = 0.$$

The values were taken approximate to the result, although they can generally be arbitrary, since the convergence to the solution with discontinuity is ensured primarily by the boundary conditions

$$h_i u_i\big|_{x=-3} = (Q_i)_{\text{in}} = \text{const}, \quad \frac{\partial h_i}{\partial x}\bigg|_{x=-3} = 0, \quad i = 1,2. \tag{65}$$

On the right, we set a fixed boundary for the depth and drift for the velocity:

$$h_1 + b\big|_{x=3} = 0.9205217, \quad h_2\big|_{x=3} = 0.5794783, \quad \frac{\partial u_i}{\partial x}\bigg|_{x=3} = 0, \quad i = 1,2. \tag{66}$$

In the numerical integration of this problem, the solution exhibits grid oscillations near the discontinuity. To smooth these spurious oscillations, by analogy with the quasi-hydrodynamic algorithm for the simulation of supersonic gas flows, the expression for the viscous stress tensor (34), (35) has to be supplemented by Navier–Stokes viscosity regularizers (57).

The numerical results at $t = 500$ are presented in Figs. 11 and 12. It can be seen that the layer distributions (Fig. 11a) and the Froude numbers (Fig. 11b) obtained on different grids nearly coincide, and the mass flux $j_i, i = 1,2$ does not differ from the exact solution in Fig. 12: $j_i = (Q_i)_{\text{in}} = \text{const}, i = 1,2$.

The results also coincide with the reference solution from [2], where the boundary depths were specified as

$$h_1\big|_{x=-3} = 1.0816731, \quad h_1\big|_{x=3} = 0.9205217,$$

$$h_2\big|_{x=-3} = 0.4311358, \quad h_2\big|_{x=3} = 0.5794783,$$

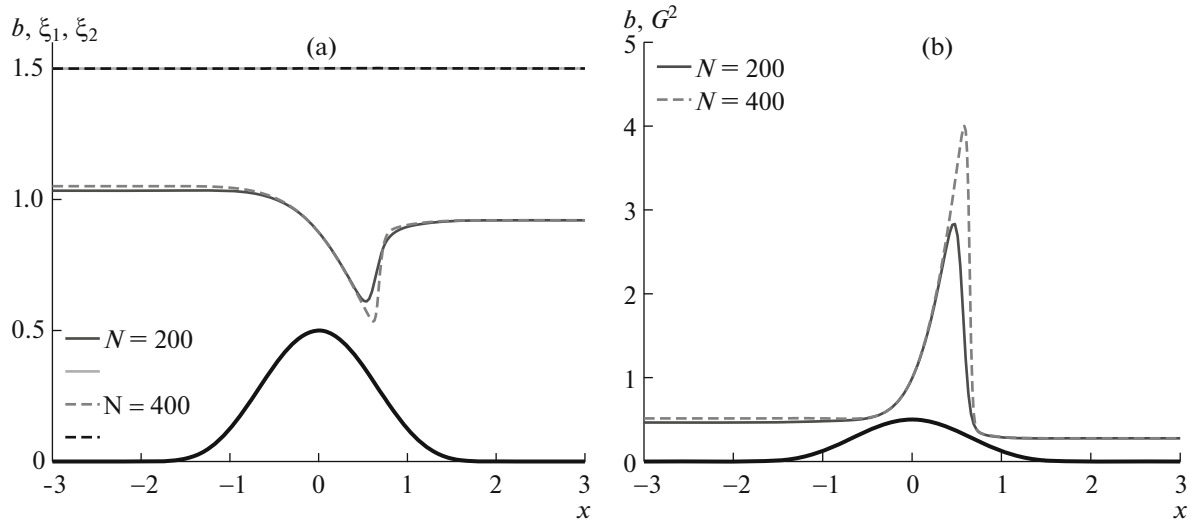and the discontinuity was localized at $x = 0.48$, as in the large system.

Fig. 11. Test 4, large system, flow with discontinuity for various N, $\alpha = 0.5$, $\beta = 0.1$, and $t = 500$: (a) layer depth distribution and (b) Froude number with schematic bottom topography.
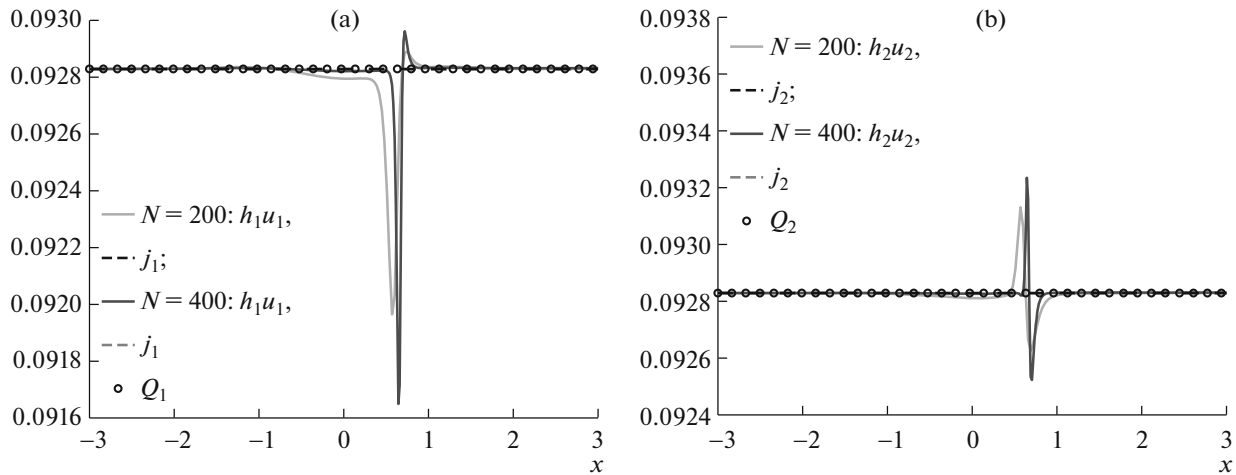

Fig. 12. Test 4, flow with discontinuity, flux distribution for various N, $\alpha = 0.5$, $\beta = 0.1$, and $t = 500$: (a) first layer and (b) second layer.

Counterflows

This problem differs only in that the flow direction in one layer is opposite to the other:

$$(Q_1)_{\text{in}} = -(Q_2)_{\text{in}} = 0.09282893.$$

The initial conditions were specified as before by (61) and (62), but the boundary conditions for the upper layer were different. Namely, on the right boundary,

$$h_2 u_2 \big|_{x=3} = (Q_2)_{\text{in}} = \text{const}, \qquad \frac{\partial h_2}{\partial x}\bigg|_{x=3} = 0, \tag{67}$$

and, on the left, we set the flow drift condition

$$\frac{\partial h_2}{\partial x}\bigg|_{x=-3} = 0, \qquad \frac{\partial u_2}{\partial x}\bigg|_{x=-3} = 0. \tag{68}$$

The boundary conditions for the lower layer were the same as before: (59) and (60) (i.e., only for $i = 1$).

The layer depth distribution in this case perfectly agrees with Fig. 10, so it is not shown. This result repeats the case of parallel flows, since the exact solution (58) is satisfied by both formulations (the solution is independent of the flow direction).

It should be noted that the problem of counterflows is unstable with respect to initial data, so the result may not converge to the desired solution. Possibly, in solving such problems, we need to take into account viscosity, which plays an important role in the interaction of counterflows. Additionally, unstable perturbations arise under mesh refinement. For this reason, regularizer (57) with coefficient $\gamma = 0.1$ was introduced into the scheme in order to reduce the oscillations.

9. EXAMPLE OF USING TWO-LAYER SHALLOW WATER EQUATIONS IN CONSERVATIVE FORM

According to the formulations in [12, 15, 25], the two-layer shallow water equations can be represented as a system of conservation laws, i.e., in conservative form. By using the notation introduced in Section 1, for one-dimensional plane flows, we can write this system as

$$\frac{\partial h_1}{\partial t} + \frac{\partial}{\partial x}(h_1 u_1) = 0, \tag{69}$$

$$\frac{\partial h_2}{\partial t} + \frac{\partial}{\partial x}(h_2 u_2) = 0, \tag{70}$$

$$\frac{\partial u_1}{\partial t} + \frac{\partial}{\partial x}\left(\frac{u_1^2}{2}\right) + g\frac{\partial}{\partial x}(h_1 + rh_2 + b) = 0, \tag{71}$$

$$\frac{\partial u_2}{\partial t} + \frac{\partial}{\partial x}\left(\frac{u_2^2}{2}\right) + g\frac{\partial}{\partial x}(h_1 + h_2 + b) = 0. \tag{72}$$

After performing transformations similar those described in Section 2, in the same notation as before, the regularized form of system (69)−(72) is written as

$$\frac{\partial h_1}{\partial t} + \frac{\partial j_1}{\partial x} = 0, \tag{73}$$

$$\frac{\partial h_2}{\partial t} + \frac{\partial j_2}{\partial x} = 0, \tag{74}$$

$$\frac{\partial u_1}{\partial t} + \frac{\partial}{\partial x}\left(\frac{u_1^2}{2}\right) + g\frac{\partial}{\partial x}(h_1 + rh_2 + b) = \frac{\partial \widetilde{\Pi_1}}{\partial x}, \tag{75}$$

$$\frac{\partial u_2}{\partial t} + \frac{\partial}{\partial x}\left(\frac{u_2^2}{2}\right) + g\frac{\partial}{\partial x}(h_1 + h_2 + b) = \frac{\partial \widetilde{\Pi_2}}{\partial x}, \tag{76}$$

$$\widetilde{\Pi_1} = \frac{1}{h_1}\Pi_1 + rg\tau_2\frac{\partial(h_2 u_2)}{\partial x}, \tag{77}$$

$$\widetilde{\Pi_2} = \frac{1}{h_2}\Pi_2 + g\tau_1\frac{\partial(h_1 u_1)}{\partial x}, \tag{78}$$

here, w_1, j_1, w_2, j_2, Π_1, and Π_2 are given by formulas (30)−(35), respectively.

Inspection of the regularized conservative system shows that the first two equations coincide with (26) and (27), while the velocity equations are simpler than those in the large system, i.e., (28), (29). Applying

identity transformations, we can show that momentum equations (28) and (29) differ from Eqs. (75) and (76) by the term $h_i A_i$, where

$$A_1 = 2\frac{\partial(h_1 u_1)}{\partial x}\frac{\tau_1}{h_1}\left[\frac{\partial}{\partial x}\left(\frac{u_1^2}{2}\right) + g\frac{\partial}{\partial x}(h_1 + rh_2 + b)\right],$$

$$A_2 = 2\frac{\partial(h_2 u_2)}{\partial x}\frac{\tau_2}{h_2}\left[\frac{\partial}{\partial x}\left(\frac{u_2^2}{2}\right) + g\frac{\partial}{\partial x}(h_1 + h_2 + b)\right].$$

This term is proportional to τ_i and, due to its structure, vanishes for smooth stationary solutions of the original system of equations.

To estimate the effectiveness of system (73)−(78) for numerical simulation, following the approach presented in Section 3, we constructed a difference scheme and ran it as applied to the problems described above. It was shown that system (73)−(78) satisfies the hydrostatic equilibrium conditions. The results obtained in Tests 2 and 3 were found to agree well with the reference solutions. However, we failed to simulate the transcritical flow problem (Test 4), i.e., to obtain a discontinuous solution.

It should be noted that the computation times for the regularized system considered in this section are somewhat less than for system (26)−(35).

Thus, the numerical computations of the test problems performed with the conservative system show that these two approaches differ little as applied to the tests under study. This conclusion confirms the well-known fact that, in cases of practical interest, limiting discontinuous solutions based on the nonconservative shallow water equations differ little from solutions of the conservative equations. An example of such a comparison for the Saint Venant equations for an actual channel can be found in [27].

CONCLUDING REMARKS

As the main result of this work, a new time-explicit difference scheme for the simulation of two-layer shallow water flows was constructed, and its performance was tested.

The method was found to be stable in the case where the upper layer density is only slightly lower than that in the lower layer. Such values are typical of oceanic flows of various salinity and temperature. Examples are the currents in the Strait of Gibraltar and tidal internal waves within it [3, 5]. It was also shown that the algorithm is applicable to flows with widely different layer densities and flows with internal dry-bed zones, which suggest that it can be used to simulate tsunami waves generated by an underwater landslide [5, 28]. The generalizations of the algorithm to two dimensions are straightforward and can be checked using the tests described in [6, 7, 9].

APPENDIX

Small System

The large system is derived assuming that the velocity and depth of a layer change to take new values $\mathbf{u}^*$ and h^*, respectively.

The small system, which is a simplified regularizer, takes into account variations in the velocity, but neglects depth variations:

$$\mathbf{u}^* = \mathbf{u} + \tau\frac{\partial\mathbf{u}}{\partial t}.$$

The regularization of Eqs. (15)−(18) by this method yields the following system, which was described in [19]:

$$\frac{\partial h_1}{\partial t} + \operatorname{div}\mathbf{j}_1 = 0,$$

$$\frac{\partial h_2}{\partial t} + \operatorname{div}\mathbf{j}_2 = 0,$$

$$\frac{\partial (h_1 \mathbf{u}_1)}{\partial t} + \mathrm{div}\,(\mathbf{j}_1 \otimes \mathbf{u}_1) + \nabla \frac{gh_1^2}{2} + gh_1 \nabla\,(rh_2 + b) = \mathrm{div}\,\Pi_1,$$

$$\frac{\partial (h_2 \mathbf{u}_2)}{\partial t} + \mathrm{div}\,(\mathbf{j}_2 \otimes \mathbf{u}_2) + \nabla \frac{gh_2^2}{2} + gh_2 \nabla\,(h_1 + b) = \mathrm{div}\,\Pi_2,$$

where

$$\mathbf{w}_1 = \tau_1 \left[(\mathbf{u}_1 \cdot \nabla)\,\mathbf{u}_1 + g\nabla\,(h_1 + rh_2 + b)\right],$$

$$\mathbf{j}_1 = h_1\,(\mathbf{u}_1 - \mathbf{w}_1),$$

$$\mathbf{w}_2 = \tau_2 \left[(\mathbf{u}_2 \cdot \nabla)\,\mathbf{u}_2 + g\nabla\,(h_1 + h_2 + b)\right],$$

$$\mathbf{j}_2 = h_2\,(\mathbf{u}_2 - \mathbf{w}_2),$$

$$\Pi_1 = (\Pi_{NS})_1 + h_1 \mathbf{u}_1 \otimes \mathbf{w}_1,$$

$$\Pi_2 = (\Pi_{NS})_2 + h_2 \mathbf{u}_2 \otimes \mathbf{w}_2,$$

here, $(\Pi_{NS})_i$, $i = 1, 2$, is the Navier–Stokes viscosity regularizer (57).

The derivation of the equations in the one-dimensional case is described in detail in [26].

ACKNOWLEDGMENTS

REFERENCES

1. F. Bouchut and T. Morales de Luna, "An entropy satisfying scheme for two-layer shallow water equations with uncoupled treatment," ESAIM: Math. Model. Numer. Anal. **42** (4), 638−698 (2008).

2. R. Abgrall and S. Karni, "Two-layer shallow water system: a relaxation approach," SIAM J. Sci. Comput. **31** (3), 1603−1627 (2009).

3. M. J. Castro, J. Macias, and C. Pares, "A Q-scheme for a class of systems of coupled conservation laws with source term: Application to a two-layer 1-D shallow water system," ESAIM: Math. Model. Numer. Anal. **35** (1), 107−127 (2001).

4. M. J. Castro, A. Pardo, C. Pares, and E. F. Toro, "On some fast well-balanced first order solvers for nonconservative systems," Math. Comput. **79** (271), 1427−1472 (2010).

5. M. J. Castro, J. A. Garcia-Rodriguez, J. M. Gonzalez-Vida, J. Macias, C. Pares, and M. E. Vazquez-Cendon, "Numerical simulation of two-layer shallow water flows through channels with irregular geometry," J. Comput. Phys. **195** (1), 202−235 (2004).

6. A. Kurganov and G. Petrova, "Central-upwind schemes for two-layer shallow water equations," SIAM J. Sci. Comput. **31** (3), 1742−1773 (2009).

7. K. T. Mandli, "A numerical method for the two layer shallow water equations with dry states," Ocean Model. **72**, 80−91 (2013).

8. A. Chertock, A. Kurganov, Z. Qu, and T. Wu, "On a three-layer approximation of two-layer shallow water equations," Math. Model. Anal. **18** (5), 675−693 (2013).

9. S. C. Chen and S. H. Peng, "Two dimensional numerical model of two-layer shallow water equations for confluence simulation," Adv. Water Resources **29**, 1608−1617 (2006).

10. V. V. Ostapenko, "Numerical simulation of wave flows caused by a shoreside landslide," J. Appl. Mech. Tech. Phys. **40** (4), 647−654 (1999).

11. V. V. Ostapenko, "Method for theoretical estimation of imbalances in nonconservative difference schemes on a shock wave," Dokl. Akad. Nauk SSSR **295** (2), 292−297 (1987).

12. L. V. Ovsyannikov, "Two-layer shallow water model," J. Appl Mech. Tech. Phys. **20** (2), 127−135 (1979).

13. V. Yu. Lyapidevskii and V. M. Teshukov, *Mathematical Models of Long Wave Propagation in an Inhomogeneous Fluid* (Sib. Otd. Ross. Akad. Nauk, Novosibirsk, 2000) [in Russian].

14. V. V. Ostapenko, "Complete systems of conservation laws for two-layer shallow water models," J. Appl. Mech. Tech. Phys. **40** (5), 796−804 (1999).

15. V. V. Ostapenko, "Stable shock waves in two-layer shallow water," J. Appl. Math. Mech. **65** (1), 89−108 (2001).

16. B. N. Chetverushkin, *Kinetically Consistent Schemes in Gas Dynamic* (Mosk. Gos. Univ., Moscow, 1999) [in Russian].

17. Yu. V. Sheretov, *Continuum Dynamics under Spatiotemporal Averaging* (NITs Regulyarnaya i Khaoticheskaya Dinamika, Moscow, 2009).

18. T. G. Elizarova, *Quasi-Gas Dynamic Equations* (Nauchnyi Mir, Moscow, 2007; Springer-Verlag, Berlin, 2009).

19. O. V. Bulatov and T. G. Elizarova, "Regularized shallow water equations and an efficient method for numerical simulation of shallow water flows," Comput. Math. Math. Phys. **51** (1), 160−173 (2011).

20. O. V. Bulatov and T. G. Elizarova, "Regularized shallow water equations for numerical simulation of flows with a moving shoreline," Comput. Math. Math. Phys. **56** (4), 661−679 (2016).

21. O. V. Bulatov, "Analytical and numerical Riemann solutions of the Saint Venant equations for forward- and backward-facing step flows," Comput. Math. Math. Phys. **54** (1), 158−171 (2014).

22. Yu. V. Sheretov, *Regularized Fluid Dynamic Equations* (Tver. Gos. Univ., Tver, 2016) [in Russian].

23. A. A. Zlotnik, "On conservative spatial discretizations of the barotropic quasi-gasdynamic system of equations with a potential body force," Comput. Math. Math. Phys. **56** (2), 303−319 (2016).

24. A. A. Samarskii and Yu. P. Popov, *Finite Difference Methods for Problems in Gas Dynamics* (Nauka, Moscow, 1975) [in Russian].

25. P. E. Karabut and V. V. Ostapenko, "Problem of the decay of a small-amplitude discontinuity in two-layer shallow water: First approximation," J. Appl. Mech. Tech. Phys. **52** (5), 698−688 (2011).

26. T. G. Elizarova and A. V. Ivanov, "Quasi-gas dynamic algorithm for the numerical solution of two-layer shallow water equations," Preprint No. 691, IPM RAN (Keldysh Institute of Applied Mathematics, Russian Academy of Sciences, Moscow, 2016).

27. M. V. Buntina and V. V. Ostapenko, "TVD scheme for computing open channel wave flows," Comput. Math. Math. Phys. **48** (12), 2241−2253 (2008).

28. B. W. Levin and M. A. Nosov, *Physics of Tsunamis* (Yanus-K, Moscow, 2005; Springer, Berlin, 2008).

Translated by I. Ruzanova